

Development of Control Strategies for the Joined-Wing Aircraft

Bernardo Cunha

Instituto Superior Técnico,

Av. Rovisco Pais 1, 1049-001 Lisboa, Portugal

(Dated: June 6, 2011)

Keywords: Joined-Wing, SensorCraft, Unmanned Aerial Vehicle, Mixed-control, Speed-brake control, Automatic Flight Control System

Abstract

Different control strategies for the Joined-Wing SensorCraft are developed and analyzed, for which the prime objective is the control of this rudderless aircraft configuration. The aircraft stability coefficients were determined through the combine effort of AVL (Athena Vortex Lattice) and XFOIL programs, allowing for the static and dynamic stability to be analyzed. Based on previous stability results and coefficients several configurations were designed to control the yaw motion. Using the Control System Theory two evaluation methods were created to compare the several configurations and to control the aircraft motion. Finally, the most efficient configuration to control the yaw motion was obtained.

I. INTRODUCTION

The Joined-Wing SensorCraft belongs to a new generation of High-Altitude Long-Endurance (HALE) aircrafts of Unmanned Aerial Vehicles (UAVs) family. This aircraft is a merging between stealth, endurance and a low-band array, able to provide 360° coverage [1]. Its unusual configuration incorporates two wings in which the forward wing is swept back positive dihedral to join the aft wing, which is swept forward anhedral, forming a diamond arrangement [2]. This configuration was created with the purpose of integrate a new type of radar as a part of the airframe, increasing the sensing capability [1].

A. Geometry

The SensorCraft has ten control surfaces along the forward and aft wings. Six control surfaces are located in the forward wing and the other four in the aft wing. The distribution of the control surfaces is shown in FIG. 1 and

the TABLE I makes the matching between the designation used for each control surface and the code assigned to it. Symmetrical right and left control surfaces (CS) are defined by the same code.

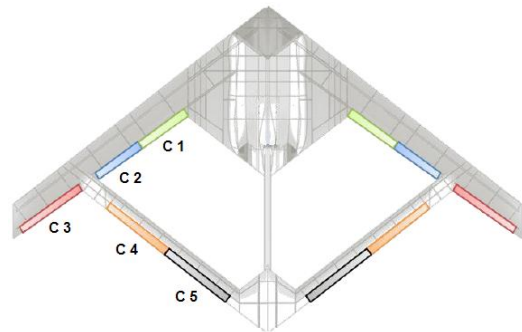


FIG. 1. SensorCraft control surfaces distribution.

TABLE I. Legend of FIG. 1.

Control Surface	Code
Flaps	C1
Inboard Ailerons	C2
Outboard Ailerons	C3
Outboard Elevators	C4
Inboard Elevators	C5

B. Objectives

The objective of this work is the stability analysis and the development of strategies to control the aircraft motion, but mainly the yaw motion due to the lack of a rudder.

C. Methods

It will be analyzed two different methods to achieve the yaw control. One based on the combination of the available control surfaces in both wings, in order to produce a yawing moment. It is defined as mixed-control (MC).

The other method is defined as speed-brake control (SBC) and its objective is to work as an aerodynamic brake in the wings, creating a differential drag force [3] between them and therefore a yawing moment.

II. DYNAMICS OF FLIGHT

A. Equations of Motion

The Euler's Equations of Motion, which describe the aircraft flight, were written in the Stability Axis [4] using the Small Disturbance Theory [4].

As simplification it was admitted the following trim conditions, as usually done in Automatic Flight Control System (AFCS) studies:

- Straight flight;
- Symmetric flight;
- Flying with wings leveled;
- Trimmed flight.

B. State Space Representation

To analyze the equations of motion it was chosen the state space representation as following:

$$\dot{x} = Ax + Bu, \quad (1)$$

where, x is the vector representing the state variables, u is the vector representing the control input variables, A represent the state coefficient matrix and B represents the driving matrix.

Therefore, the equations of longitudinal and lateral motion are represented by:

$$\begin{bmatrix} \dot{u} \\ \dot{w} \\ \dot{q} \\ \dot{\theta} \end{bmatrix} = \begin{bmatrix} X_u & X_w & 0 & -g \cos \gamma_0 \\ Z_u & Z_w & Z_q + U_0 & -g \sin \gamma_0 \\ \tilde{M}_u & \tilde{M}_w & \tilde{M}_q & \tilde{M}_\theta \\ 0 & 0 & 1 & 0 \end{bmatrix} \begin{bmatrix} u \\ w \\ q \\ \theta \end{bmatrix} + \begin{bmatrix} X_{\delta_{s1}} & X_{\delta_{s2}} \\ Z_{\delta_{s1}} & Z_{\delta_{s2}} \\ M_{\delta_{s1}} & M_{\delta_{s2}} \\ 0 & 0 \end{bmatrix} \begin{bmatrix} \delta_{s1} \\ \delta_{s2} \\ \vdots \end{bmatrix}, \quad (2)$$

$$\begin{bmatrix} \dot{\beta} \\ \dot{p} \\ \dot{r} \\ \dot{\phi} \\ \dot{\psi} \end{bmatrix} = \begin{bmatrix} Y_\beta & \frac{Y_p}{U_0} & \left(\frac{Y_r}{U_0} - 1\right) & \left(\frac{g}{U_0} \cos \gamma_0\right) & 0 \\ L_\beta & L_p & L_r & 0 & 0 \\ N_\beta & N_p & N_r & 0 & 0 \\ 0 & 1 & \tan \gamma_0 & 0 & 0 \\ 0 & 0 & \sec \gamma_0 & 0 & 0 \end{bmatrix} \begin{bmatrix} \beta \\ p \\ r \\ \phi \\ \psi \end{bmatrix} + \begin{bmatrix} \frac{Y_{\delta_{s1}}}{U_0} & \frac{Y_{\delta_{s2}}}{U_0} \\ L_{\delta_{s1}} & L_{\delta_{s2}} \\ N_{\delta_{s1}} & N_{\delta_{s2}} \\ 0 & 0 \\ 0 & 0 \end{bmatrix} \begin{bmatrix} \delta_{s1} \\ \delta_{s2} \\ \vdots \end{bmatrix}, \quad (3)$$

where, u and w are the longitudinal and vertical velocities respectively, p , q and r are rolling, pitching and yawing angular velocities respectively, X , Y and Z are the longitudinal, lateral and vertical forces respectively, L , \tilde{M} and N are the rolling, pitching and yawing moments respectively, β , θ , ϕ and ψ are the sideslip, pitching, bank and yawing angles respectively, U_0 is the upstream air speed, γ_0 is the reference flight path angle and δ_s is the deflection angle of the control surface.

The infinitely variables δ_{s_n} represent the number of control inputs possible to add to the system.

The notation X_i represent the stability derivatives and it is defined as:

$$X_i = \frac{1}{m} \frac{\partial X}{\partial i}, \quad (4)$$

where, m is the aircraft mass.

III. STABILITY COEFFICIENTS

The stability coefficients are the result of the adimensionalization of the stability derivatives. Its notation is exemplified for the stability derivative in equation (4) as shown below:

$$C_{X_i}. \quad (5)$$

A. AVL Simulation

The AVL program is a 3-D numerical Computational Fluid Dynamics (CFD) code which uses the Vortex Lattice Method to analyze the stability coefficients of the aircraft [5].

The SensorCraft was discretized into several lifting surfaces as shown in FIG. 2, and the stability coefficients determined [6].

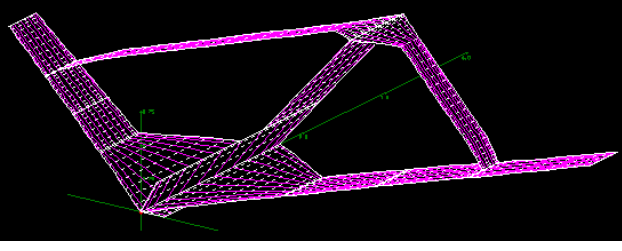


FIG. 2. AVL discretized model of SensorCraft.

B. Drag Contribution

The drag contributions are many, but the most important to the subsonic SensorCraft are:

- Induced drag
- Parasitic Drag
 - Profile drag
 - Skin friction drag

Since AVL uses an inviscid flow analysis, the induced drag is computed, but the parasitic drag contributions are neglected. Thus, it was decided to use the viscous analysis program XFOIL.

The objective is to determine both components of drag coefficient (C_D) due to the deflection of the control surfaces, induced drag coefficient (C_{D_i}) and parasitic drag coefficient (C_{D_p}), which will have much importance to the speed-brake control strategy.

Therefore, the drag coefficient variation with the control surface deflection ($C_{D_{\delta_s}}$) must be calculated for the several drag contributions, using AVL for the induced drag coefficient ($C_{D_{i_{\delta_s}}}$) and XFOIL for the parasitic drag coefficient ($C_{D_{p_{\delta_s}}}$) contribution. The XFOIL uses a 2-D analysis, for that reason the 3-D effects of induced drag do not exist, and results can be merged.

C. Method

For each control surface the process was to compute the values of C_D for given values of δ_s . $C_{D_{\delta_s}}$ is determined by the slope of the linear interpolation of the curve C_D vs δ_s . This curve has always a parabolic shape, thus it was considered two intervals. One interval defining the $C_{D_{\delta_s}}$

of the decreasing codomain, and the other defining the $C_{D_{\delta_s}}$ of the increasing codomain.

As a result, each control surface will have two values of $C_{D_{\delta_s}}$ depending on the direction of the deflection of the control surface.

The FIG. 3 represents the typical variation of C_{D_p} with δ_s , for the control surface C3, as well as the respective positive and negative curve slopes.

Therefore, using this method for XFOIL and AVL calculations, it was determined the coefficients $C_{D_{p_{\delta_s}}}$ and $C_{D_{i_{\delta_s}}}$, respectively.

D. Results and Implications

The more precise values of $C_{D_{\delta_s}}$ are given by the contributions of $C_{D_{i_{\delta_s}}}$ and $C_{D_{p_{\delta_s}}}$, in the following expression:

$$C_{D_{\delta_s}} = C_{D_{i_{\delta_s}}} + \left(\frac{U_{0n}}{U_0}\right)^2 C_{D_{p_{\delta_s}}}, \quad (6)$$

where, U_{0n} is the upstream air speed normal to the airfoil due to the wing sweep angle [6].

Since the new contribution of drag acts on the horizontal plane of the Stability Axis [4], it will produce an additional component in the yawing moment coefficient due to the CS deflection ($C_{n_{\delta_s}}$). This contribution is given by:

$$C_{n_{\delta_s}} = -\frac{l_y}{b} C_{D_{\delta_s}} + \frac{l_x}{b} C_{Y_{\delta_s}}, \quad (7)$$

where, b is the wingspan, l_y is the distance of the CS to the X-axis and l_x is the distance of the CS to the Y-axis [6].

IV. AIRCRAFT STABILITY

A. Static Stability

The static stability defines the aircraft ability of returning to the initial equilibrium condition after a force or moment disturbance has been applied. Depending on the

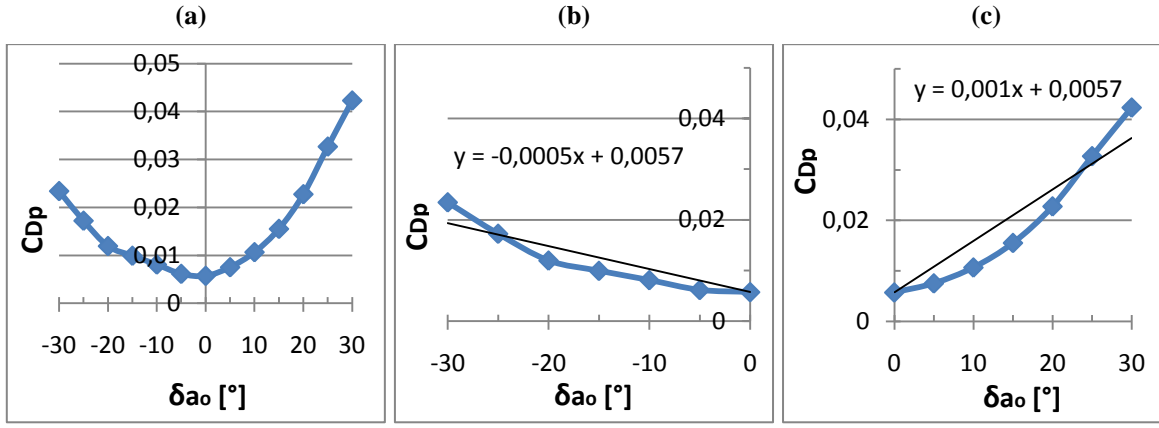


FIG. 3. (a) Variation of C_{D_p} with δ_s for the control surface C3 (b) Linear interpolation of the decreasing codomain of C_{D_p} with δ_s for the control surface C3 (c) Linear interpolation of the increasing codomain of C_{D_p} with δ_s for the control surface C3.

aircraft response (if it returns to the equilibrium or not) it can be classified as: statically stable, unstable or neutral.

The analysis of the static stability parameters resulted in an aircraft statically stable as shown in TABLE II.

TABLE II. Static stability evaluation of SensorCraft.

Static Stability		
Specification	Value	Result
$M_w < 0$	-0,48	Stable
$X_u < 0$	-0,02	Stable
$Z_w < 0$	-3,73	Stable
$Y_\beta < 0$	-0,17	Stable
$N_\beta > 0$	0,55	Stable
$L_\beta < 0$	-19,9	Stable

B. Dynamic Stability

The dynamic stability is the reduction of the disturbance in time. It is analyzed determining the eigenvalues of the state coefficient matrix A for both longitudinal and lateral motions, as shown in equation (8).

$$|\lambda I - A| = 0, \quad (8)$$

where, λ is the eigenvalues, and I is the identity matrix.

The analysis of the eigenvalues determines the dynamic stability parameters, such as, the damping ratio ξ , the natural frequency ω_n , the period of oscillation P , time constant T_R and time to double the amplitude T_2 .

Those parameters are essential to qualify the longitudinal and lateral modes, through the comparison with flying quality specification tables [4]. The results for the longitudinal and lateral modes are given in TABLE III.

TABLE III. Dyanmic stability of the aircraft longitudinal and lateral modes.

Mode	Eigenvalue	Result
Short Period	$-4,24 \pm 3,37i$	level 1
Phugoid	$0,011 \pm 0,5i$	unstable
Spiral	-0,01	level 1
Dutch roll	$-0,09 \pm 1,9i$	level 2
Roll	-6,3	level 1

In resume, the longitudinal motion is unstable because of the phugoid mode, since the longitudinal level quality is the worst of the two longitudinal modes.

The lateral motion was determined as level 2 by the flying quality of the dutch roll mode. This is unusual for common aircrafts where the spiral mode tends to be unstable and of worst quality than the dutch roll. However, this unusual but expected characteristic is related to the SensorCraft non-existence of a vertical stabilizer, which plays a huge role in dutch roll mode.

C. Overall Evaluation

From the analysis of the longitudinal dynamic stability and the stability coefficients results, it was easily seen that the control surfaces C5 are the ones which have a greater contribution in the pitching moment. In that way, C5 are the most promising control surfaces to feedback the longitudinal system and increase the dynamic stability.

On the other hand, the lateral dynamic stability indicates the need of a rudder to increase the very low dutch roll damping ratio ($\xi = 0,047$).

From the study of the stability coefficients and aerodynamic analysis, the elevators C4 and C5 are the control surfaces which most contribute for the yawing moment, and then capable of controlling it. However, activating only this CS in the same direction creates only a pitching moment (cancelling the yawing moment), or in the opposite directions creates the yawing moment but also a rolling moment. Therefore, the solution was obtained with the combination of C4 and C5 in aft wing with the C1, C2 and C3 in front wing. The FIG. 4 represents the combined use of a front wing CS (C3) and an aft wing CS (C4). Notation of positive (+) and negative (-) is adopted to represent the downwards and upwards deflection of CS, respectively.

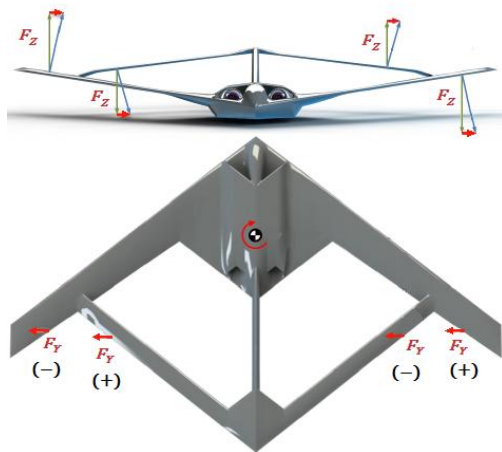


FIG. 4. Representation of the incremental forces produced by the deflection of C3 and C4 in front and top views. C3 are working as ailerons (deflecting down in the right wing and up in the left wing) and C4 are working as ailerons but in opposite direction (up in the right wing and down in the left wing). The vertical components of force tend to cancel each other and lateral force components contribute for the same yawing moment.

Using this evaluation results, it was concluded that although elevators have the greater influence in yaw, they have to be combined with front wing CS to cancel the rolling moment and even resulting in a same direction yawing moment.

Therefore, different testing configurations were designed, representing the strategies of mixed-control and speed-brake control, in order to compare their efficiency to control the yawing moment. Two configurations used

representing the different strategies are presented in FIG.5 and FIG. 6.

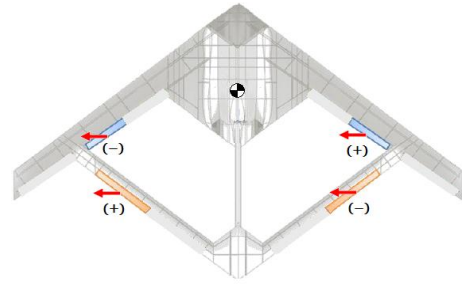


FIG. 5. Mixed-control configuration 1, using C2 and C4 in opposite directions. The red arrow represents the lateral force component produced by the respective CS deflections.

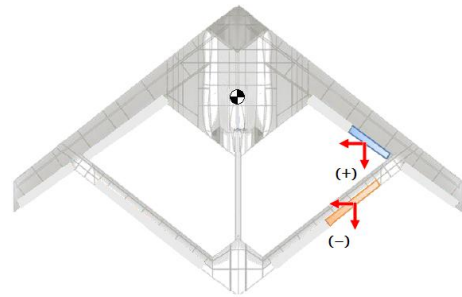


FIG. 6. Speed-brake configuration 1. The CS deflections are activated separately in either left or right wing depending in which wing is needed to brake. C2 and C3 have opposite deflections for the same reason of mixed-control of cancelling the rolling moment. Since left side is not producing drag, two components now produce the yawing moment, the longitudinal drag force and the lateral force.

The other configurations followed the same principles and are presented in FIG. 7 and FIG. 8.

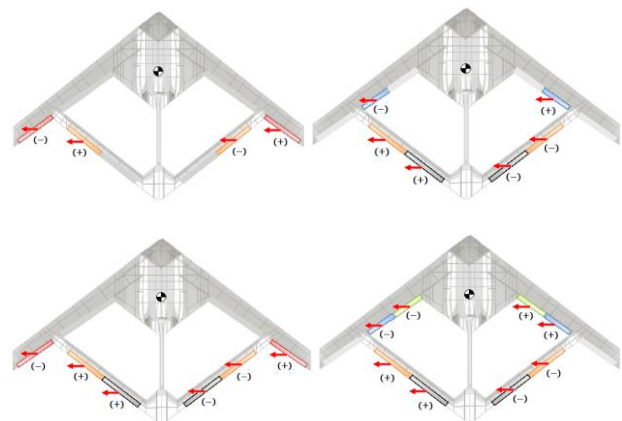


FIG. 7. Other mixed-control test configurations

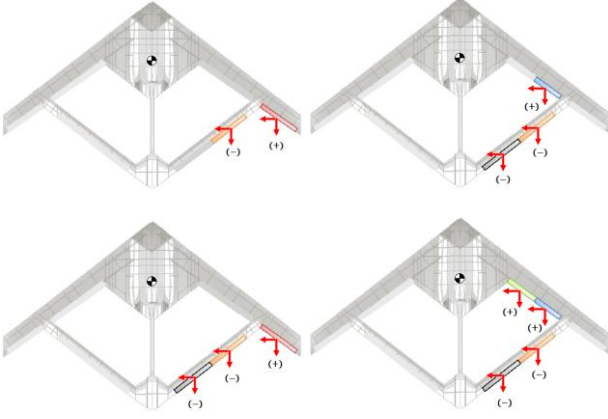


FIG. 8. Other speed-brake test configurations

V. CONTROL SYSTEM

A. Equivalent Rudder Control Surface

The use of a large number of control surfaces can lead to several solutions and not all of them feasible. Therefore, it was proposed to simplify the degrees of freedom, establishing physic relations between the control surfaces, transforming into equivalent conventional control surfaces.

For example, the right and left elevators if deflected in same direction, they act like an equivalent elevator for which the longitudinal stability coefficients are given by the sum of both elevators, while the lateral stability coefficients tend to cancel each other. The inverse happens, when using the left and right ailerons deflecting in opposite directions.

Consequently, assuming a linear interval of $[-30^\circ, 30^\circ]$, where the operations between the different stability coefficients are linear, we can transform each configuration of mixed-control and speed-brake control into an equivalent rudder.

In order to calculate the equivalent rudder stability coefficients, the optimization process aimed firstly for the minimization of the rolling moment, and only after for the maximization of the yawing moment. This way each complex yaw configuration was transformed into a conventional equivalent rudder, simplifying the degrees of freedom.

B. Control System Theory

The control system theory is based in the feedback control, where the system uses the measurement of the output state variables to rectify the control action (input controls). Thus:

$$u = Kx . \quad (9)$$

where, K is the matrix of the gain which defines the feedback.

Replacing equation (9) into equation (1), we obtain the new state matrix of the feedback system, given by:

$$\dot{x} = (A + BK)x . \quad (10)$$

C. Conventional Control System

The conventional control system chosen to design the stability augmentation was the root locus. This is a graphical method which analyzes the result of the feedback for several values of gain.

For the longitudinal mode the solution that enhanced the phugoid and short period mode qualities was following feedback for the elevators C5:

$$\delta_e = K_q q , \quad (11)$$

$$\delta_e = K_\theta \theta . \quad (12)$$

where, δ_e is the deflection of control surface C5, K_q and K_θ are they gain values.

The root locus representation for the above feedback is given in FIG. 9.

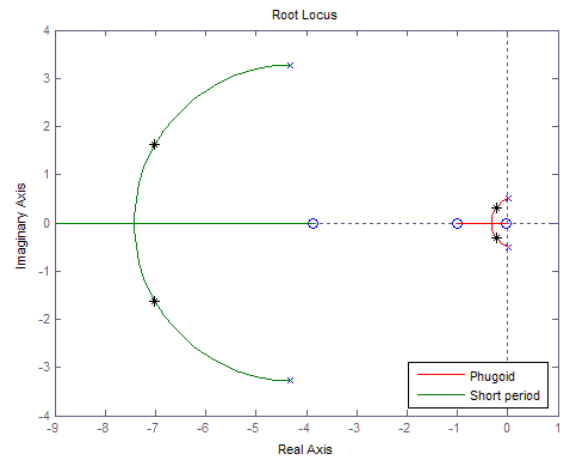


FIG. 9. Longitudinal root locus for the feedback in equations (11) and (12)

The feedback in equations (11) and (12) successfully stabilized the longitudinal model, and the previous unstable phugoid accomplish level 1 quality.

For the lateral motion, the speed-brake configuration 1 was chosen to be tested in the root locus analysis. To stabilize the lateral mode dutch roll, it was used the following feedback:

$$\delta_r = K_r r. \quad (13)$$

The root locus of this feedback is given in FIG. 10.

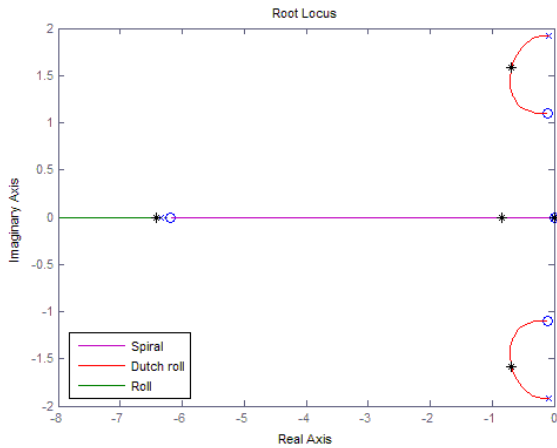


FIG. 10. Lateral root locus for the feedback in equation (13)

The chosen feedback greatly increased the flying qualities of the dutch roll mode, achieving level 1. Also because of the good behave of the chosen feedback the spiral qualities are increased, and the roll mode practically did not change.

D. Root Locus Configurations Comparison

The root locus comparison has the objective of analyzing the gains between configurations. The gain value reflects the amount of effort required from a control surface to stabilize the motion, as shown in equation (9).

To grant a fair comparison, the gain values of the different configurations were calculated to reach the same eigenvalues. Thus, the gains represent the effort of a configuration to achieve the same flying qualities.

The gain result obtained for the different configurations is represented in FIG. 11.

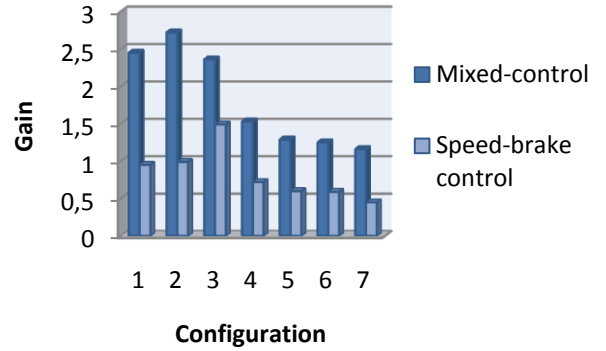


FIG. 11. Gain values for mixed and speed-brake control configurations

E. Modern Control Methods

The modern method used was the Linear Quadratic Regulator (LQR) which leads to the optimal controller using an all state and input variables feedback.

The feedback gain matrix is determined minimizing the cost function, J , defined as equation (14):

$$J = \int_{t_1}^{t_2} \mathcal{L}(x, u, t) dt, \quad (14)$$

where, J is the cost function and \mathcal{L} is the Lagrangian which summarizes the dynamic of the system [4].

This method was applied only to the lateral motion, since all the longitudinal modes successfully increased their flying qualities with root locus.

The objective is to build a flight path system in which the aircraft can follow a certain request in the yawing angle. To eliminate the static errors in the bank and yawing angles it was introduced the integrative terms of these states, in equation (3), using the following form:

$$\dot{x}_6 = \phi, \quad (15)$$

$$\dot{x}_7 = \psi. \quad (16)$$

The computed gain matrix increased the dynamic stability of all lateral modes, with more efficiency than the root locus. Thus, all modes achieved level 1 flying quality.

The system will be tested to an extreme change in the heading angle ψ of 90° and for a command in the bank angle to level the wings after the perturbation.

Therefore, the inputs of the flight path control system are:

$$\psi^{com} = 90^\circ \quad (17)$$

$$\phi^{com} = 0 \quad (18)$$

The ψ^{com} input is activated at the marked time of 10s after the simulation started.

In order to simulate a precise control maneuver it were applied limit constraints to the bank angle of 10° , The FIG. 12 represents the variation of the state variables after the command input given in equations (17) and (18) for the speed-brake configuration 1.

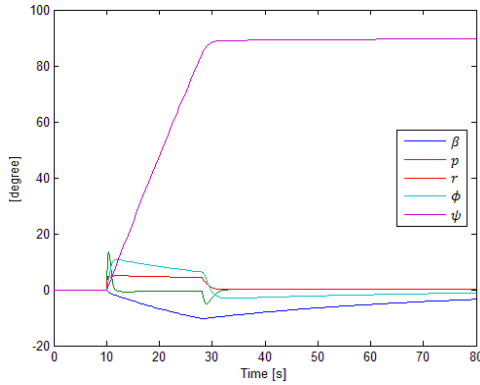


FIG. 12. Response of LQR feedback system

F. LQR Configurations Comparison

The objective is now to use the previous LQR feedback system to investigate the different control configurations. The comparison between the several configurations will be done based on the heading angle state variable ψ , through the analysis of the time to accomplished the requested input.

The fair comparison between configurations is granted by using the same pondering matrices which minimized the cost function, stabilizing the first configuration analyzed. The results obtained for the mixed-control and speed-brake control configurations are presented in FIG. 13 and FIG. 14, respectively.

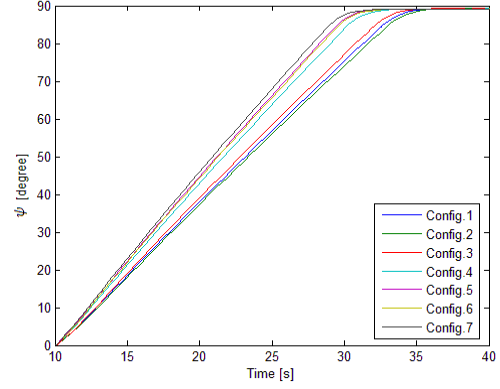


FIG. 13. Time to complete the turn of 90° by mixed-control configurations

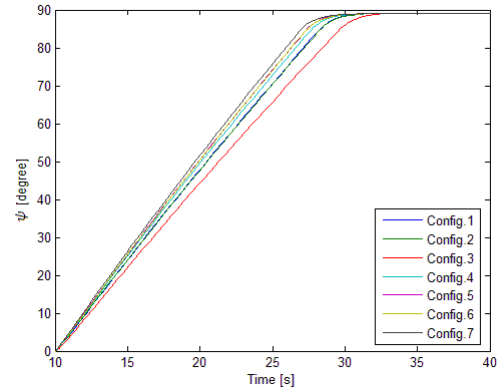


FIG. 14. Time to complete the turn of 90° by speed-brake control configurations

In FIG. 15 the comparison of mixed-control and speed-brake control configurations results clarifies the differences between them.

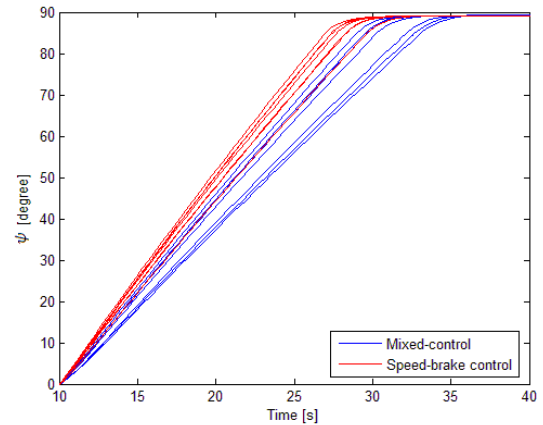


FIG. 15. Mixed-control and speed-brake control configuration comparison

VI. QUALITATIVE VALIDATION WITH THE SENSORCRAFT HEURISTIC MODEL

Since we do not have access to experimental results and in order to validate the conclusions obtained in this work, a qualitative comparison was done with the flight tests results from a heuristic model, that was being developed simultaneously in another thesis [7].

The Joined-Wing heuristic model was build with the following material: foam (roofmate) as main material; glass and carbon fibres materials as reinforcements of the main frame [7].



FIG. 16. Joined Wing SensorCraft 3 [7]

After the construction and the installation of all electronic equipment, the model was submitted to several flight tests controlled via radio. All the results obtained were based in the qualitative aircraft observation and pilot feedback of the control configurations applied.

Therefore, from the qualitative data was possible to evaluate the yaw control strategies, through a qualitative

scale system. The configuration which received more points was the speed-brake control configuration 1[7].

VII. CONCLUSIONS

From the various control strategies and after several investigations using: feedback systems, computation and analysis of stability coefficients, and flight path control systems, we came to the conclusion that mixed-control strategies have inferior results than speed-brake control strategies to control the aircraft yaw.

The speed-brake control configurations which better control the aircraft yaw were configurations 1 and 6. These two configurations stand out because of their significant efficiency to control the lateral motion, and at the same time they do not decrease the autonomy of the aircraft rolling motion and pitching motion (pitching only respected by configuration 1).

Between configurations 1 and 6, an increase of the yawing stability coefficient of 38% for configuration 6 was observed. Nevertheless it involves the use of twice the number of control surfaces. Therefore, the use of each configuration will depend on the flight condition, precision and aircraft real environment situations.

The flight tests for the Joined-Wing heuristic model resulted in a qualitatively superior yaw control for the speed-brake configurations instead of the mixed-control configurations, and the speed-brake configuration 1 demonstrated higher qualities in controlling the yaw motion. Therefore the flight test results showed a strong agreement with the theoretical results.

References

[1] Trimble, Stephen, *“Over the Horizon”*, Flight International publication, Wright Patterson Air Force Base, Ohio, July 2005.

[2] Snyder, R., Hur, J., Strong, D., and Beran, P. S., *“Static Aeroelastic Analysis of a High-Altitude Long-Endurance Joined-Wing Aircraft”*, Structural Dynamics, and Materials Conference, Austin, April 2005.

- [3] Cazals, O., Druot, T., "Aircraft with yaw control by differential drag", US Patent 12/847108, March 2011.
- [4] McLean, D., *Automatic Flight Control Systems*, Prentice Hall, 1990.
- [5] Anderson, J. D., *Fundamentals of aerodynamics*, 2nd Ed., McGraw-Hill, 1991.
- [6] Cunha, B., *Development of Control Strategies for the Joined-Wing Sensorcraft*, Master Thesis, Universidade Técnica de Lisboa – Instituto Superior Técnico, June 2011.
- [7] Antunes, Luis, *Design and Manufacturing of a Joined-Wing Experimental Flight Demonstrator*, Master Thesis, Universidade Técnica de Lisboa – Instituto Superior Técnico, June 2011.